

Kinetics of H atom attack on unsaturated hydrocarbons using spectral uncertainty propagation and minimization techniques

David A. Sheen^{1,2}, Claudette M. Rosado-Reyes² and Wing Tsang²

¹*Department of Mechanical and Aerospace Engineering, University of Virginia,
Charlottesville, VA 22904, USA*

²*National Institute of Standards and Technology, Gaithersburg, MD 20899, USA*

Corresponding Author:

David A. Sheen

National Institute of Standards and Technology

Mail Stop 8320

Gaithersburg, MD 20899-8320, USA

david.sheen@nist.gov

Colloquium: Reaction Kinetics

Word Count (Method 1)

Main Body	3842
Figure 1 (13.11 mm x 2 col + 16 words in caption)	118
Figure 2 (4.06 mm x 2 col + 80 words in caption)	142
Figure 3 (4.06 mm x 2 col + 47 words in caption)	109
Figure 4 (4.191 mm x 2 col + 73 words in caption)	135
Figure 5 (4.04 mm x 1 col + 89 words in caption)	120
Figure 6 (6.38 mm x 1 col + 40 words in caption)	76
Table 1 (25 lines x 2 col + 3 words in caption)	413
Table 2 (31 lines x 2 col + 6 words in caption)	508
References (32)	594
Equations (5, 7 lines)	129
Total	6186

Abstract 278

Keywords: Combustion kinetics, Modeling, Uncertainty analysis, Unsaturated hydrocarbons, Pyrolysis

Submitted for consideration at the 34th International Symposium on Combustion, Warsaw
University of Technology, Warsaw, Poland, July 29th – August 3rd, 2012

Kinetics of H atom attack on unsaturated hydrocarbons using spectral uncertainty propagation and minimization techniques

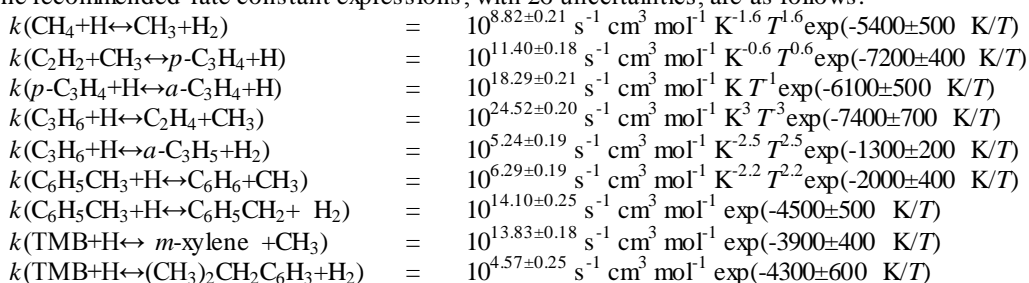
David A. Sheen^{1,2}, Claudette M. Rosado-Reyes² and Wing Tsang²

¹*Department of Mechanical and Aerospace Engineering, University of Virginia,
Charlottesville, VA 22904, USA*

²*National Institute of Standards and Technology, Gaithersburg, MD 20899, USA*

Abstract

Unsaturated hydrocarbons are an important component of hydrocarbon fuels and intermediates in their oxidation. Under rich conditions, H atom attack is one of the principal pathways of the decomposition of these unsaturated compounds. Consequently, it is critical to understand the H atom attack mechanisms as part of chemical model development. Previous studies have examined the kinetics of H atom attack on various unsaturated hydrocarbons in single pulse shock-tubes. These studies have noted that there are multiple pathways by which H atom attack can proceed, so it is straightforward to measure relative rates but absolute rates are more difficult to estimate. In addition, there is a confounding influence from secondary chemistry. A multiparameter optimization and uncertainty minimization technique is used to constrain a chemical model for the oxidation of H₂/CO/C₁-C₄ hydrocarbons against a range of measurements of the H atom attack process on toluene, trimethylbenzene (TMB), propyne, and propene. The recommended rate constant expressions, with 2σ uncertainties, are as follows:



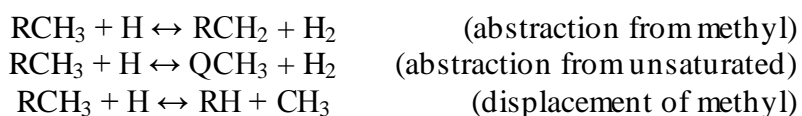
In addition, we quantify the effect of secondary chemistry on these rate estimates and the contribution to their uncertainty. Furthermore, we demonstrate how the detailed measurements constrain the model's predictions of global properties such as ignition delay time in propene oxidation.

1. Introduction

Hydrocarbon fuels commonly used in the transportation industry contain a significant fraction of unsaturated and aromatic species. In addition, unsaturated species such as propene are intermediates in the pyrolysis and oxidation of saturated hydrocarbons. Consequently, understanding the formation and decomposition mechanisms of these compounds is a critical part of the development of a chemical kinetics model for oxidation of fuels. In addition, it is

necessary to quantify the uncertainties inherent in the model in order to propagate them into simulations of interest, such as engine performance and emissions predictions.

Under fuel-rich conditions, the primary pathway for the decomposition of unsaturated compounds is via H-atom attack, which has been studied in single-pulse shock tubes [1-4]. These studies have demonstrated that there are multiple pathways by which H atom attack can proceed, which can make the analysis difficult [1-8]. An unsaturated methylated hydrocarbon attacked by an H atom can experience either abstraction of an H atom or displacement of the methyl group, i.e.



In experiments performed by Tsang and co-workers [1-4], some substances, either hexamethylethane (HME) or *t*-butylperoxide (tBPO), were used as an H atom source. HME decomposes into two *t*-butyl radicals, and these release an H atom and an isobutene molecule. The isobutene concentration is therefore a measure for how many H atoms are released into the system. Likewise, the concentration of RH can be directly measured; the ratio between these two values measures the displacement rate and the total abstraction rate. Alternatively, an experiment can be performed with two species simultaneously such that the concentration ratio between $\text{R}_{(1)}\text{H}$ and $\text{R}_{(2)}\text{H}$ is a measure of the displacement rate for these two species.

Compiling a chemical kinetics model, such as for combustion in an engine, requires that a rate expression be specified for each reaction in the model. For the ratio of rate constants to be useful, therefore, it is necessary to know at least one of the rate constants. Other researchers were aware of this fact and performed some measurements in the presence of methane [1, 2].

Under this condition, the rate constants for H-atom attack on toluene and 1,3,5-trimethylbenzene (TMB) were fixed relative to the rate constant for R126, $\text{CH}_4 + \text{H} \leftrightarrow \text{CH}_3 + \text{H}_2$ which was well-known. Subsequent studies [3, 4] measured H-atom attack rates on propene and propyne relative to those on TMB, so that all of these rate constants are coupled to k_{126} . Each of these measurements has some uncertainty in it, which will introduce uncertainty in the rate constant estimates. Due to the complex chain of dependence of one rate constant on measurements of another, the uncertainties of all the rate constants will be tied together in some fashion that is not trivial to calculate.

Furthermore, secondary chemistry can influence the rate constant estimates. For instance, H can recombine with the RCH_2 radical, thereby increasing the total apparent abstraction rate. This effect was quantified for the rate constants of H-atom attack on toluene [2] and determined to be less than the experimental uncertainty. Other molecules could participate in more interesting chemistry, however. Propyne, for instance, can isomerize to allene upon attack by an H atom. It can also undergo unimolecular isomerization, which has been observed to have a strong effect at high temperatures [3]. Some chemistry models, such as JetSurF [9], also consider propyne isomerization to allene moderated by the propargyl radical. Consideration of these pathways, and their effect on rate constant determination from the single-pulse shock tube measurements, would allow for more accurate estimates of the rate constants and their uncertainties over a wider range of conditions.

The goal of the present study is to determine the kinetics of H-atom attack on unsaturated hydrocarbons using the previously-proposed Method of Uncertainty Minimization using Polynomial Chaos Expansions (MUM-PCE). This method was originally developed to constrain a detailed chemical model against a wide variety of combustion phenomena, including laminar

flame speeds and ignition delay [10-13] as well as detailed species measurements in shock tube oxidation [12, 14]. MUM-PCE is part of a class of methods including DataCollaboration [15-17] and model updating [18-21]. In these methods, a chemical model is compiled which describes the chemical processes to be simulated in as much detail as possible. As part of the compilation process, the uncertainty in the rate parameters must be specified. In Bayesian terminology, this is the prior model. Experiments that will be used to constrain the model are then simulated. Based on these simulations, a set of possible rate parameter values is identified whose corresponding predictions agree with the experimental measurements; this is called the feasible region [15-17], and the corresponding model is called the posterior model. Model updating [18-21] and MUM-PCE [10-14] use a statistical approach that determines a credible region and a probability density function on that credible region. Model updating involves selecting a representative random sample of possible models within the credible region. MUM-PCE determines the probability density function directly from the derivatives of simulated measurements with respect to the model rate parameters.

In this paper, we conduct a detailed analysis of H atom attack on several unsaturated hydrocarbons. Experimental data are used for toluene [1], TMB [2], propyne ($p\text{-C}_3\text{H}_4$) [3], and propene [4]. We combine all of the experimental data together and use it to constrain a complete model for the pyrolysis and oxidation of H_2 , CO, and the $\text{C}_1\text{-C}_4$ hydrocarbons. We characterize the uncertainty of the model based on the constraints provided by the experimental data and propagate this uncertainty into simulations of the oxidation of propyne.

2. Methodology

2.1. Reaction model

The chemical model used here is based on the JetSurF 2.0 large alkane oxidation model [9]. This model provides the reaction rate and thermochemical parameters for $\text{H}_2/\text{CO}/\text{C}_1\text{-C}_4/\text{toluene}$ oxidation, and has been extensively validated against a wide range of combustion data. In addition, reaction models were added for TMB [2], HME [1], tBPO [22], and ethylbenzene [23]. Thermochemical parameters for species not in JetSurF were taken from [24]. The thermochemical parameters of *iso*-octane were used for HME, since the two compounds have similar enthalpies and entropies at the temperatures under consideration, and the concentrations are so low that heat release from HME decomposition is not significant. The complete model consists of 124 species and 819 reactions and is given in the supplementary material, along with associated uncertainty factors for all reaction rates.

As is usual in combustion, the reaction model specifies rate constants as a function of temperature in the usual three parameter Arrhenius form, $k_n(T) = A_n T^{b_n} \exp(E_n/T)$, with some uncertainty factor F_n . The index n runs over the total number of reactions N , but not every rate parameter will be constrained. The number of reactions to which any particular simulation is sensitive is usually much less than N . Uncertainty of b_n is not considered, since many values of b_n have no uncertainty. Some reactions, such as recombination reactions, are written as barrierless reactions with $E = 0$. Therefore, the number of parameters to be constrained is not $3N$ but some smaller number I , shown later. The A and E values selected to be constrained are reordered into a vector of active variables $\boldsymbol{\theta}$ and a vector of factorial variables $\mathbf{x}^{(0)}$. Each $x_i^{(0)}$ is related to each uncertain model parameter θ_i by the relation

$$x_i^{(0)} = \frac{\ln \theta_i / \theta_{i,0}}{\ln f_i} \quad (1)$$

where $\theta_{i,0}$ is the nominal value of the i^{th} uncertain parameter and f_i is the (2σ) uncertainty factor for that parameter. The factorial variables are convenient to work with because if $x_i^{(0)} = \pm 1$, θ_i is at its upper or lower bound. Values of f_i for A 's are equal to the corresponding F_n and taken from the supplemental information in [10]. For most reactions this is approximately 2. Values of f_i for E 's were chosen by the relation $\ln f_i = (E_n + T_c \ln F_n) / E_n$, with $T_c = 1000$ K. To account for the possibility of small E , f_i was set to a maximum of 1.2.

The factorial variables are assumed to follow a multivariate normal distribution, which implies that there is a random factorial vector $\mathbf{x} = \mathbf{x}^{(0)} + \mathbf{x}^{(1)T} \boldsymbol{\xi}$. Here, $[]^T$ denotes the transpose operator and $\boldsymbol{\xi}$ is a vector of independent, identically distributed (iid) normal random variables with mean 0 and variance 1. In the case of the prior model, we take $\mathbf{x}^{(1)}$ to be equal to $\mathbf{1}/2$, where $\mathbf{1}_I$ is the I -element identity matrix; likewise, we take $\mathbf{x}^{(0)} = \mathbf{0}$.

2.2. Experimental data and simulation details

Conditions for the experimental measurements used are detailed in Table 1. Some measurements, noted in the table, are used for validation only, because of strong correlations between similar experiments. Each measured species concentration ratio has a functional relationship with the rate constant ratio for a pair of H-atom attack reactions, as detailed in [1-4]. Uncertainties in the measured species concentration ratios were taken to be 10% (2σ) as estimated in [3, 4]. The shock tube was simulated as an unsteady 0-dimensional batch reactor with initial conditions as specified in Table 1 and run for 500 μs . Calculations used the VODE solver [25] to integrate the chemical rate equations supplied by Sandia CHEMKIN [26].

In order to reduce the computational complexity, problems of this type are usually solved using the solution mapping method [27, 28]. In this method, the model predictions η are expressed as polynomials with respect to the factorial variables,

$$\eta_r(\mathbf{x}^{(0)}) = \mathbf{x}^{(0)T} \mathbf{b}_r \mathbf{x}^{(0)} + \mathbf{a}_r^T \mathbf{x}^{(0)} + \eta_{0,r} \quad (2)$$

where \mathbf{a}_r and \mathbf{b}_r are the first- and second-order derivatives of the r^{th} model prediction, η_r , with respect to $\mathbf{x}^{(0)}$. These derivatives were calculated using the brute-force sensitivity-analysis-based method (SAB) [29]. For each prediction there is also an observed value η_r^{obs} and its corresponding uncertainty σ_r^{obs} , taken to be 10% as estimated in [3, 4].

I was determined based on the sensitivity of the constraining experiments, as detailed in [12]. For each simulated experiment r and each parameter j of the total number of possible parameters $J = 2N$, a normalized sensitivity $D_{r,j} = f_j S_{r,j}$ is calculated, where $S_{r,j}$ is the logarithmic sensitivity coefficient of the r^{th} model prediction with respect to the j^{th} parameter. Then, for each simulated experiment, all rate parameters with $D_{r,j}/D_{r,\max}$ greater than some D_{\min} are chosen as active. In this case, $D_{\min} = 0.02$, resulting in $I = 57$. The reaction rate parameters selected by this process are shown in Table 2. Further references to specific reactions in this paper use the form RN , and k_n , A_n , or E_n for its corresponding rate constant and rate parameters.

2.3. Uncertainty minimization

The uncertainty minimization procedure used here (MUM-PCE) is described in [11, 13], and summarized briefly here. Once the experimental constraints have been chosen, there must be some posterior model that best reproduces those experimental measurements, which has a corresponding \mathbf{x} denoted as $\mathbf{x}^* = \mathbf{x}^{(0)*} + \mathbf{x}^{(1)*} \boldsymbol{\xi}$. As discussed in [13], the uncertainties in the experimental measurements and the rate constant estimates are assumed to be normally

distributed about their mean values. This lends itself to estimating \mathbf{x}^* using least-squares minimization; \mathbf{x}^* therefore corresponds to the mode (and mean) of a multivariate-normal probability density function. $\mathbf{x}^{(0)*}$ is determined using maximum likelihood, which is equivalent to solving the least-squares problem,

$$\Phi(\mathbf{x}^{(0)*}) = \min_{\mathbf{x}^{(0)}} \sum_{r=1}^M \left(\frac{\eta_r(\mathbf{x}^{(0)}) - \eta_r^{\text{obs}}}{\sigma_r^{\text{obs}}} \right)^2 + \sum_{i=1}^I 4x_i^{(0)2} \quad (3)$$

where M is the number of experimental constraints, η_r^{obs} is the mean measurement for the r^{th} constraint, and σ_r^{obs} is its measured uncertainty. $\mathbf{x}^{(1)}$ is calculated by linearizing the polynomial functions in the vicinity of $\mathbf{x}^{(0)*}$, $\eta_r^* = \mathbf{J}_r \mathbf{x}^{(0)*}$, where \mathbf{J}_r is the gradient of the r^{th} polynomial. Then, the covariance matrix among the rate parameters is

$$\Sigma = \mathbf{x}^{(1)} \mathbf{x}^{(1)T} = \left(\sum_{r=1}^M \frac{\mathbf{J}_r \mathbf{J}_r^T}{\sigma_r^{\text{obs}}} + 4\mathbf{I} \right)^{-1} \quad (4)$$

3. Results and discussion

3.1. Constraint on reaction rate parameters

It is to be expected that the most sensitive reactions will be those for displacement of CH_3 by H from the parent molecule and abstraction of H by H to form the resonantly-stabilized radical. The low value of D_{min} , and the reaction rate parameters that are chosen because of it, allow exploration of the secondary pathways that might be important for these experiments. The list of reactions chosen by the screening process is given in Table 2, along with the corresponding $\mathbf{x}^{(0)*}$ values, and the results are mostly as expected. Propyne pyrolysis has unusual behavior

because R320, $p\text{-C}_3\text{H}_4 + \text{H} \leftrightarrow \text{C}_3\text{H}_3 + \text{H}_2$ has an extremely low rate at 1000 K; instead, the strong sensitivity is to R316, $p\text{-C}_3\text{H}_4 + \text{H} \leftrightarrow a\text{-C}_3\text{H}_4 + \text{H}$ and R315, $p\text{-C}_3\text{H}_4 \leftrightarrow a\text{-C}_3\text{H}_4$, consistent with what was observed in [3]. Secondary pathways selected include reactions such as R321, $p\text{-C}_3\text{H}_4 + \text{C}_3\text{H}_3 \leftrightarrow a\text{-C}_3\text{H}_4 + \text{C}_3\text{H}_3$ and R556, $1\text{-C}_4\text{H}_8 + \text{H} \leftrightarrow \text{C}_3\text{H}_6 + \text{CH}_3$. The effects of these pathways will be discussed below.

The two main results of the optimization study are $\mathbf{x}^{(0)*}$ and $\mathbf{\Sigma}^*$, which are shown in Table 2 and Fig. 1 respectively; a complete listing of posterior rate expressions and uncertainty factors is given in Table S1. A rate parameter's $x_i^{(0)*}$ indicates how adequate the rate coefficients of the prior model are for simulating the experiments. A_{126} and E_{126} have small values of $x_i^{(0)*}$, meaning that the experiments can be simulated accurately without changing these coefficients.. A_{362} , on the other hand (corresponding to R362, $\text{C}_3\text{H}_6 + \text{H} \leftrightarrow \text{C}_2\text{H}_4 + \text{CH}_3$), has a very large and positive $x_i^{(0)*}$, while the $x_i^{(0)*}$ for E_{362} is large and negative, indicating that k_{362} must be faster over the relevant temperature range by several factors, relative to the prior model, to reproduce the measurements of these experiments. The condition number κ of $\mathbf{\Sigma}^*$ gives a broad measure of how much information about the system is obtained from the experimental measurements and also of the accuracy of $\mathbf{\Sigma}^*$; for this system, $\kappa = 1000$, so the credible region is very flat in at least one direction, and $\mathbf{\Sigma}^*$ is accurate to one part in 10^{13} . The $\mathbf{\Sigma}^*$ values associated with a reaction rate parameter indicate how much information is contained within the chosen experiments about that rate parameter. For most rate parameters, the standard deviation, $\Sigma_{ii}^{*1/2}$, is close to 0.5 and the covariances, Σ_{ij}^* , are close to 0; these are not shown in Fig. 1. E_{674} (corresponding to R674, $\text{C}_6\text{H}_5\text{CH}_3 + \text{H} \leftrightarrow \text{C}_6\text{H}_6 + \text{CH}_3$) has a $\Sigma_{ii}^{*1/2}$ of 0.45, but some values of Σ_{ij}^* are significantly greater than 0. For instance, the $\Sigma_{ij}^{*1/2}$ between A_{674} and E_{674} is nearly 0.3, since choosing a certain E

constrains the choices for A that will reproduce the experimental measurements. This means that the temperature dependence of k_{674} has not been uniquely identified, but its value is constrained based on values other parameters might take. Conversely, A_{674} has a $\Sigma_{ii}^{*1/2}$ of 0.25, indicating that it has been measured more precisely.

The Σ_{ij}^* values for R674 can be compared with those for R814, $\text{TMB} + \text{H} \leftrightarrow m\text{-xylene} + \text{CH}_3$. Experiments measuring the reactivity of H with toluene, which were used to determine k_{674} , were only taken over a relatively narrow temperature range [1], as can be seen in Table 1. These measurements can determine a reaction's A value very precisely, but not its E value. In the case of A_{814} and E_{814} , the $\Sigma_{ii}^{*1/2}$ for both parameters is relatively small (0.2 and 0.3, respectively) because the measurements using TMB in [3, 4] contain information about the behavior of $\text{TMB} + \text{H}$ over a wider temperature range than the measurements of [2]. Note that the rate parameters for all of the principal reactions are coupled to R126, which is expected since that reaction was used as the standard in [1, 2]. The small Σ_{ii}^* ($\Sigma_{ii}^{*1/2} \approx 0.35$) and large Σ_{ij}^* ($\Sigma_{ij}^{*1/2} \approx 0.3$) for these parameters indicates that these experiments determine a precise value for k_{126} ; there are values of A_{126} , for instance, which would make it impossible to explain the observed data. The presence of R321 and R355, and their nonzero Σ_{ij}^* values, indicates pathways that produce significant amounts of products in ways that are difficult to isolate. The effect of these reactions will be noted later.

To illustrate the effects of constraining the rate constants using experimental measurements, k_{673} and k_{674} are presented in Fig. 2. Included in the figure are the prior model uncertainty based on the estimates of [30], the posterior uncertainty which includes the measurements in Table 1, and the rate expressions calculated in [1]. The posterior model uncertainty is much smaller than the prior model uncertainty, and as indicated in Fig. 1. This is because of constraint on the A

values. As expected, the values for the posterior model rate constants agree with [1], but the mean activation energy is significantly different, so that extrapolating the rate constants to much higher or lower temperatures will give very different values. This illustrates the utility of a method such as MUM-PCE, because not only the uncertainty in the rate constant at the temperature at which it was measured is known but that uncertainty can be extrapolated over the entire range where the prior model estimate is valid, 400 K – 2000 K [30].

3.2. Constraint on experimental measurements

In addition to the rate constants, it is also possible to examine the uncertainty in the model predictions and the corresponding effects from secondary chemistry. In the previous studies of Tsang and co-workers [1-4], functional relationships were derived between the ratios of certain product species and the pathways that produce them. As an example, $[i\text{-C}_4\text{H}_8]/[\text{C}_6\text{H}_6]$ for Series 1-1 (see Table 1 for conditions) and the abstraction to displacement rate constant ratio, k_{673}/k_{674} , are shown in Fig. 3. The measured product ratio is taken directly from [1] and the measured rate ratio is estimated from the functional relationship proposed in [1]. The prior model uncertainty is much larger than the measurement uncertainty, while the posterior model uncertainty is equal to the measurement uncertainty, as expected. Similarly, the posterior model calculation goes straight through the measured $[i\text{-C}_4\text{H}_8]/[\text{C}_6\text{H}_6]$ values, which is expected since the model was constrained against these data. On the other hand, the predicted k_{673}/k_{674} is less than the estimated value by about 10% at higher temperature, indicating that there is less C_6H_6 produced than would be expected. The result can be explained by R680, by which benzyl radicals siphon H atoms from the system. This is a similar conclusion to the one reached in the re-analysis from [2].

The same measurement was performed for propene [4], which is included as Series 4-3 in Table 1; the results are presented in Fig. 4. The uncertainty in the measured $[i\text{-C}_4\text{H}_8]/[\text{C}_2\text{H}_4]$ is assumed to be 10%, and the propagated uncertainty in the rate constant ratio is about 50%. Unlike the case for toluene, the $[i\text{-C}_4\text{H}_8]/[\text{C}_2\text{H}_4]$, measured experimentally, lies at the edge of the prior model's uncertainty band; this explains the very large change in the posterior values for A_{362} and E_{362} presented in Table 2. It is still possible, however, to generate a posterior model that agrees with the experimental measurements, as shown in the figure. The posterior abstraction to displacement rate constant ratio, however, is about 50% larger than that calculated using the functional relationship, as can be seen in the figure, meaning that more C_2H_4 is produced than would be expected. It was noted above that R556 appears in Fig. 1 as coupled to R363; this reaction can produce H atoms without $i\text{-C}_4\text{H}_8$, so they will not be properly counted.

3.3. Validation of the constrained model

Once the posterior model has been determined, the uncertainty of the prior and posterior models can be propagated into some simulation of interest. As an example, simulations of the ignition delay time of 3.2% propene/7.8% oxygen/argon mixtures are shown in Figs. 5 and 6, along with the corresponding measurements from [31]. The reactions shown in Table 2 are only those relevant to the H-atom attack experiments, and as such, the simulations of an oxidative process such as ignition delay time are sensitive to a larger set of reactions. Figure 5, therefore, shows a comparison of two possible prior models. One model considers uncertainty in the ignition delay times from only the reactions in Table 2, while the other considers that from all reactions in the model. The latter is necessarily larger than the former, by a factor of 3 at the higher temperatures, increasing to an order of magnitude at the lower temperatures. At low temperatures, the production of O atoms, such as by $\text{H} + \text{O}_2 \leftrightarrow \text{O} + \text{OH}$ and $\text{CH}_3 + \text{O}_2 \leftrightarrow \text{O} +$

CH_3O , is the principal rate-limiting process, which is a part of the hydrocarbon oxidation mechanism that the H-atom attack measurements do not constrain. As the temperature increases, the sensitivity of the simulations to O production rate constants decreases, and the H-atom reactions become more important. However, across the temperature range shown here for this system, the uncertainty from these reactions is still a relatively small portion of the total uncertainty, so that any improvements from measuring them will be washed out by the remaining uncertainty in the model.

Even if the H-atom attack reactions represent only a relatively small contribution to the total uncertainty in the oxidation process, the reduction in that contribution can still be measured. This is presented in Fig. 6, which compares ignition delay predictions for the prior and posterior models, considering uncertainty from only the reactions in Table 2. At low temperatures the uncertainty of the posterior model is the same as the prior model, which indicates that the H-atom attack measurements do not shed any light on the propene oxidation process at this temperature. With increasing temperature, however, the posterior model uncertainty is reduced considerably, thereby indicating that the H-atom attack measurements are strongly relevant to propene oxidation process at higher temperatures.

It should be noted that the “high” temperature in Fig. 6 is 1600 K; for comparison, the highest temperature at which the rates of H-atom attack are constrained is 1200 K [3]. This underscores the utility of the method, because as long as the uncertainty in any measurement at any temperature is known, that uncertainty can then be propagated to any other temperature at which the model’s rate expressions are valid.

4. Conclusions

A model for the oxidation and pyrolysis of H_2 , CO, C_1 - C_4 hydrocarbons, toluene, and benzene was constrained against a set of measurements of the H-atom attack process on toluene, 1,3,5-trimethylbenzene, propyne, and propene in single-pulse shock tubes using the Method of Uncertainty Minimization using Polynomial Chaos Expansions (MUM-PCE). These measurements were successfully used to produce an optimized model and to calculate uncertainties in the chemical rate parameters. Secondary chemistry was found to change the determined the H-atom attack rates by an amount comparable to the experimental measurement uncertainty, particularly for propene and propyne.

In addition, the constraint of the single-pulse shock tube measurements on ignition delay time of propene was calculated. The contribution to the uncertainty in the ignition delay simulations from the H-atom attack process is reduced considerably. However, the contribution to the uncertainty from the oxidation reactions is still so high that the single-pulse shock tube measurements do not appreciably reduce the total uncertainty in the simulations. Consequently, more precise measurements of these oxidation reactions are needed.

Disclaimer

The identification of any commercial product or trade name does not imply endorsement or recommendation by the National Institute of Standards and Technology.

References

1. D. Robaugh, W. Tsang, J. Phys. Chem 90 (1986), 4159-4163.
2. W. Tsang, J. P. Cui, J. A. Walker, International Symposium on Shock Waves and Shock Tubes 17 (1989), 63-73.
3. C. M. Rosado-Reyes, J. A. Manion, W. Tsang, J. Phys. Chem. A 114 (2010), 5710-5717.
4. C. M. Rosado-Reyes, J. A. Manion, W. Tsang, J. Phys. Chem. A 115 (2011), 2727-2734.
5. I. A. Awan, D. R. Burgess Jr, W. Tsang, J. A. Manion, Proc. Combust. Inst. 33 (2011), 341-349.
6. I. A. Awan, W. S. McGivern, W. Tsang, J. A. Manion, J. Phys. Chem. A 114 (2010), 7832-7846.
7. W. S. McGivern, I. A. Awan, W. Tsang, J. A. Manion, J. Phys. Chem. A 112 (2008), 6908-6917.
8. W. S. McGivern, J. A. Manion, W. Tsang, J. Phys. Chem. A 110 (2006), 12822-12831.
9. H. Wang, E. Dames, B. Sirjean, D. A. Sheen, R. Tangko, A. Violi, J. Y. W. Lai, F. N. Egolfopoulos, D. F. Davidson, R. K. Hanson, C. T. Bowman, C. K. Law, W. Tsang, N. P. Cernansky, D. L. Miller, R. P. Lindstedt, A high-temperature chemical kinetic model of *n*-alkane (up to *n*-dodecane), cyclohexane, and methyl-, ethyl-, *n*-propyl and *n*-butyl-cyclohexane oxidation at high temperatures, JetSurF version 2.0. <http://melchior.usc.edu/JetSurF/JetSurF2.0>; 2010
10. D. A. Sheen, X. You, H. Wang, T. Løvås, Proc. Combust. Inst. 32 (2009), 535-542.
11. D. A. Sheen. Spectral Optimization and Uncertainty Quantification in Combustion Modeling. University of Southern California, Los Angeles, CA, 2011.
12. D. A. Sheen, H. Wang, Combust. Flame 158 (2011), 645-656.
13. D. A. Sheen, H. Wang, Combust. Flame (In press), doi:10.1016/j.combustflame.2011.05.010.
14. R. Tangko, D. A. Sheen, H. Wang, in: *7th Joint Meeting of the U.S. Sections of the Combustion Institute*, Atlanta, GA, 2011.
15. M. Frenklach, A. Packard, P. Seiler, R. Feeley, Int. J. Chem. Kinet. 36 (2004), 57-66.
16. T. Russi, A. Packard, R. Feeley, M. Frenklach, J. Phys. Chem. A (2008),
17. P. Seiler, M. Frenklach, A. Packard, R. Feeley, Optim. Eng. 7 (2006), 459-478.
18. J. L. Beck, L. S. Katafygiotis, Journal of Engineering Mechanics 124 (1998), 455-461.
19. J. L. Beck, K.-V. Yuen, Journal of Engineering Mechanics 130 (2004), 192-203.
20. L. S. Katafygiotis, J. L. Beck, Journal of Engineering Mechanics 124 (1998), 463-467.
21. M. W. Vanik, J. L. Beck, S. K. Au, Journal of Engineering Mechanics 126 (2000), 738-745.
22. J. Manion, R. E. Huie, R. D. Levin, D. R. B. Jr., V. L. Orkin, W. Tsang, W. S. McGivern, J. W. Hudgens, V. D. Knyazev, D. B. Atkinson, E. Chai, A. M. Tereza, C.-Y. Lin, T. C. Allison, W. G. Mallard, F. Westley, J. T. Herron, R. F. Hampson, D. H. Frizzell, NIST Chemical Kinetics Database, NIST Standard Reference Database 17, Version 7.0 (Web Version), Release 1.4.3, Data version 2008.12. <http://kinetics.nist.gov/>; 2008
23. K. Narayanaswamy, G. Blanquart, H. Pitsch, Combust. Flame 157 (2010), 1879-1898.

24. E. Goos, A. Burcat, B. Ruscic, Third Millennium Thermodynamic Database for Combustion and Air-Pollution Use with updates from Active Thermochemical Tables. <http://garfield.chem.elte.hu/Burcat/burcat.html>; 2011
25. P. N. Brown, G. D. Byrne, A. C. Hindmarsh, SIAM Journal on Scientific and Statistical Computing 10 (1989), 1038-1051.
26. R. J. Kee, F. M. Rupley, J. A. Miller, *CHEMKIN-II: A FORTRAN Chemical Kinetics Package for the Analysis of Gas-Phase Chemical Kinetics*, SAND89-8009, Sandia National Laboratories: Albuquerque, NM, 1989.
27. M. Frenklach, Combust. Flame 58 (1984), 69-72.
28. M. Frenklach, H. Wang, M. J. Rabinowitz, Prog. Energ. Combust. Sci. 18 (1992), 47-73.
29. S. G. Davis, A. B. Mhadeshwar, D. G. Vlachos, H. Wang, Int. J. Chem. Kinet. 36 (2004), 94-106.
30. I. V. Tokmakov, M. C. Lin, Int. J. Chem. Kinet. 33 (2001), 633-653.
31. Z. Qin, H. Yang, W. C. Gardiner Jr, Combust. Flame 124 (2001), 246-254.

List of Supplemental Material

Table S1. Prior uncertainty factors and posterior rate expressions and uncertainty factors for reactions and rate parameters considered. Starred quantities denote posterior values. Units are mol, cm, s, and K. Activation energies are in K. Uncertainties in the rate constant coefficients is 2σ . (Table S1.doc)

Table S2. Prior rate expressions and uncertainty factors for the compete model. Units are mol, cm, s, and K. Activation energies are in K. (Table S2.xls)

Reaction model in CHEMKIN format (scheme.txt)

Thermochemistry model in CHEMKIN format (thermdat.txt)